Analysis of Power Amplifier Contribution to the Precision of Motion Systems

Analysis of Power Amplifier Contribution to the Precision of Motion Systems

Marziyeh Hajiheidari, Duo Xu, Jeroen van Duivenbode, Bas Vermulst, and Mircea Lazar
Department of Electrical Engineering, Eindhoven University of Technology
Eindhoven, The Netherlands
Email: m.hajiheidari@tue.nl, d.xu@tue.nl, j.v.duivenbode@tue.nl, b.j.d.vermulst@tue.nl, m.lazar@tue.nl

***Abstract*—In a high-precision motion system, a position controller creates an appropriate current reference signal based on a position reference trajectory. Then, power amplifiers use this reference signal to drive actuators to translate the current reference into the desired force to move the subject to the desired position. Any imperfection in the power amplifier performance adversely affects the overall positioning system accuracy. Hence, to improve the motion system's performance, the effects of power amplifier imperfections on such high-precision systems are investigated through a complete mechatronics model that combines control, mechanical and electrical aspects. Additionally, to demonstrate how the system performance can be improved by changing the control strategy, a voltage-mode cascaded current controller is applied to the power amplifier and different feedforward strategies are applied to the position loop. We demonstrate that the accuracy of position control can be improved by a factor of five by taking into account the amplifier dynamics and controller design.**

***Index Terms*—Power amplifiers, motion systems, modelling, position loop controller.**

I. Introduction

High-precision motion systems are the heart of certain types of industrial equipment and scientific instruments, such as wafer steppers, wire-and-die bonders, printers, medical imaging scanners, and high-precision microscopes [1], [2]. For these applications, accurate and fast motion is essential. For instance, Moore's law dictates that in lithography position systems the permissible positioning error halves approximately every 5 years. Thus, to keep up with Moore's law and reach ever-decreasing node sizes, the power amplifiers, which drive the actuators used in photo-lithography systems, are permitted to hold only a small (e.g. $\pm 1\%$) fraction of the total position error [2], [3]. Ideally, the power amplifier should work as a block with unity gain and a Zero Order Hold (ZOH) that follows the current reference created by the digital position loop controller. However, in practice, imperfections in the amplifier components, e.g. transistors, inductors, capacitors, or sensors, and the switching nature of the power amplifier adversely affect both dynamic and static accuracy of a precision motion system [4], [5].

Many previous studies have focused on the amplifier enhancement. For instance, Maurer et al. [5] has conducted a simulation-based analysis to improve the open-loop power amplifier output-voltage quality by selecting the most robust power converter topology and semiconductor devices. Schellekens et al. [6] and Yu et al. [7] provide analytical and numerical models of the output spectrum of the H-bridge inverter to investigate the effects of dead-time on the power amplifier switching node voltage precision. In Vermulst [8], a Hammerstein/ Wiener nonlinear structure is used to model regularly sampled Pulse-Width Modulators (PWMs) base-band harmonics, and a method is proposed to compensate for these nonlinearities. However, how these improvements on the power amplifier would affect the position loop accuracy is not answered in the aforementioned papers. There are other works focusing only on the position controller performance. For example, Verkerk et al. [9] suggest a Kalman observer to improve the low-frequency disturbance rejection and expand the control bandwidth in high precision control systems. Nonetheless, an analysis of the complete mechatronics system is lacking.

In Settels et al. [10], an innovative approach for analyzing high-precision mechatronic systems is suggested which includes electrical, mechanical and position control parts to evaluate the effects of the power amplifier on the position loop accuracy. The power amplifier gain error, gain offset, nonlinearity and bandwidth limitations are analyzed in [10], but noise and spurious signals effects are not investigated.

In this research, the mechatronics model developed in [10] is extended to include the effects of noise and spurious currents so that a more comprehensive vision of the power amplifier limitations is obtained. Moreover, instead of using the current-mode current controller in [10], a voltage-mode cascaded current controller is applied to a class-D power amplifier, and its effects on the position loop are investigated. Then, position errors related to feedforward delay are analyzed and a method for compensating for this delay using a fractional delay block in the feedforward path is presented.

II. Position Control System and Comparison Metrics

Fig. 1 illustrates the global structure of a motion control system, which comprises of a Set Point Generator (SPG), an electromechanical plant P which contains an actuator/motor and a power amplifier PA, feedback controller C_{FB}, feedforward controller C_{FF}, and a sampler with the sampling time $T_{s,pos} = 1/f_{s,pos}$. The simplified actuator is modeled as a second-order system with mass m_{act} and constant k_{act}. The estimated motor constant and mass, k_{est} and m_{est}, are included in the plant model. Since the effects of the power

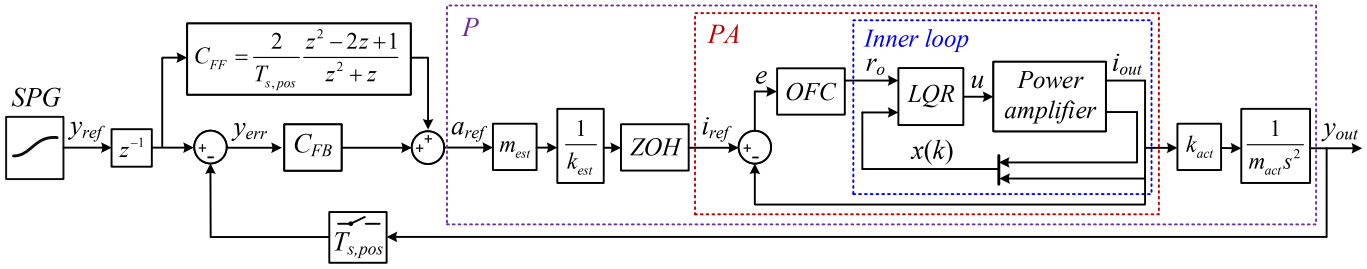

Fig. 1. Generic outline of a motion control system architecture.

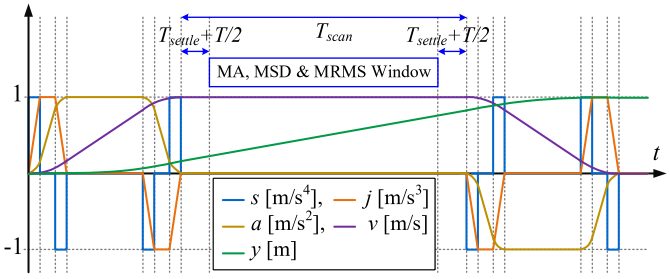

Fig. 2. Normalized representation of the fourth-order SPG.

amplifier on the motion system are investigated, k_{est} and m_{est} are taken equal to the actual motor constant and mass.

Set point generator and accuracy comparison metrics: As illustrated in Fig. 2, a fourth-order set point generator consisting of the position profile y and its consecutive derivatives including velocity v, acceleration a, jerk j, and snap s is used. The position error $y_{err}(t)$ is defined as $y_{err}(t) = y_{ref}(t) - y_{out}(t)$, where $y_{ref}(t)$ is the position reference and $y_{out}(t)$ the measured position. As demonstrated in [2], Moving Average (MA) and Moving Standard Deviation (MSD) can be used to evaluate the system performance. Peak values of |MA| and MSD are gated in an exposure window which is time-limited by the settling time T_{settle} and the slit time T. For a top-hat window, $w_{th}(t)$, the MA and MSD functions are defined as

$$MA(t) = w_{th}(t) * y_{err}(t) = \frac{1}{T}\int_{t-T/2}^{t+T/2} y_{err}(\tau)d\tau \quad (1)$$

$$\begin{aligned} MSD(t) &= \sqrt{w_{th}(t) * y_{err}^2(t) - MA^2(t)} \\ &= \sqrt{\frac{1}{T}\int_{t-T/2}^{t+T/2} (y_{err}(\tau) - MA(t))^2 d\tau}. \end{aligned} \quad (2)$$

Here, MA represents the low-frequency part of the error and is related to the system's ability to position subjects precisely on top of each other. MSD shows the high-frequency part of the error and is related to the critical dimension that a position system can achieve. Since MA is highly dependent on control loop tuning, a superior measure for the evaluation of the power amplifier contribution to the position system accuracy is Moving Root-Mean-Square (MRMS) which is defined as $MRMS(t) = \sqrt{MA(t)^2 + MSD(t)^2}$. MA, MSD, and MRMS measures are noncausal filters and are used for post-process evaluations. As Fig. 3 illustrates, in the frequency domain, MA and MSD filters act as low pass and high pass filters with a cross-over frequency $f_c = \frac{1}{2T}$. For the system evaluated in this research, the MA/MSD cross-over frequency is $f_c = 214.3$ Hz, and for digital implementation, discrete time convolutions with the sampling time $T_{s,pos} = 25$ µs are used for MA/MSD calculations.

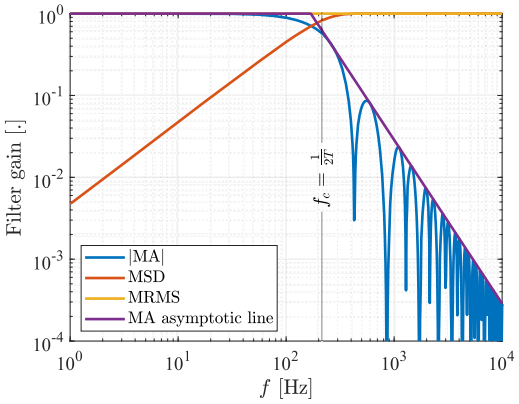

Fig. 3. MA, MSD, and MRMS frequency gains.

Feedback controller: The discrete-time feedback controller C_{FB} consists of a series connection of a PID controller, whose pure pole at the origin improves the low-frequency gain, and a second-order Low Pass Filter (LPF) which improves the system gain margin; C_{FB} is designed for an open-loop bandwidth $f_{BW,pos} = 550$ Hz, and its continuous-time transfer function is defined as

$$C_{FB}(s) = \frac{k_D s^2 + k_P s + k_I}{s} \cdot \frac{\omega_p^2}{s^2 + 2\zeta\omega_p s + \omega_p^2}, \quad (3)$$

where k_D, k_P, k_I, ω_p, and ζ are the derivative gain, proportional gain, integral gain, LPF cut-off frequency, and LPF damping factor, respectively. For digital implementation, C_{FB} is discretized with the sampling time $T_{s,pos}$.

Feedforward controller: In order to track the position reference in a fast and accurate way, a feedforward controller is included. Ideally, the transfer function of the feedforward controller should be a digital correspondent of $C_{FF} = s^2$, which is exactly the inverse of the ideal plant model $P(s)$,

considering PA as a unity gain transfer function. In this way, the feedforward controller C_{FF} converts the position reference y_{ref} to a precise system input for the plant. However, creating the exact inverse of the plant would be impossible due to the causality issue, and roll-off poles should be added into the C_{FF} to make the system causal. All the controllers are formulated in the discrete-time domain, and the reference and measured signals are sampled with $T_{s,pos}$. The ideal continuous plant model can be exactly described by the discrete-time equivalent system $P(z)$ as follows

$$P(z) = \left(1 - z^{-1}\right) \mathcal{Z}\left\{\frac{P(s)}{s}\right\}, \tag{4}$$

where $\mathcal{Z}\left\{\frac{P(s)}{s}\right\}$ denotes the z-transform of the time sequence $p(kT_{s,pos})$. The inverse of the plant $P(z)^{-1}$ has 2 zeros and 1 pole and, thus, is noncausal. To eliminate the noncausality issue, one sampling delay z^{-1} is added to both feedforward and feedback loops. Hence, the feedforward controller is reformulated as

$$C_{FF}(z) = \frac{P(z)^{-1}}{z} = \frac{2}{{T_{s,pos}}^2} \frac{z^2 - 2z + 1}{z^2 + z}. \tag{5}$$

The simulation results of the position loop setup with an ideal amplifier, unity gain with ZOH, leads to negligible position errors with a peak value of around 4×10^{-15} m. Also, the peak values of MA and MSD are around 0.011 pm and 0.051 pm, respectively.

In the following sections, MATLAB and Simulink are used to obtain MA, MSD, and MRMS errors as a function of power amplifier imperfections, which are divided in two categories: 1. additive errors and 2. current loop errors [10]. For current loop errors, the effects of the power amplifier with a cascaded current controller on the position loop are investigated.

III. Power Amplifier Additive Errors

Typically, critical additive power amplifier imperfections which adversely affect high-precision motion systems include gain drift, gain offset, nonlinearity, noise, and spurious signals. For evaluating the effects of these errors, a generic model shown in Fig. 4 is applied which is independent of the actual implementation of the power amplifier. Hence, for each current error, the position error is calculated from the sensitivity analysis in the continuous domain according as

$$y_{err} = i_{err} \cdot S_{PA} = i_{err} \cdot \frac{k_{act}}{m_{act}} \cdot \frac{P(s)}{1 + C_{FB}(s)P(s)}, \tag{6}$$

where S_{PA} is a process sensitivity which represents the position system response to the power amplifier disturbances. Since constant current offset errors are compensated by the position loop gain which is considerably high at low frequencies, gain offset is excluded from the analysis.

Gain error: The results of MA, MSD, and MRMS position errors for an amplifier gain error ranging from -0.05 A/A to $+0.05$ A/A is illustrated in Fig. 5 (a). The obtained results show that even small values of gain drift cause considerable

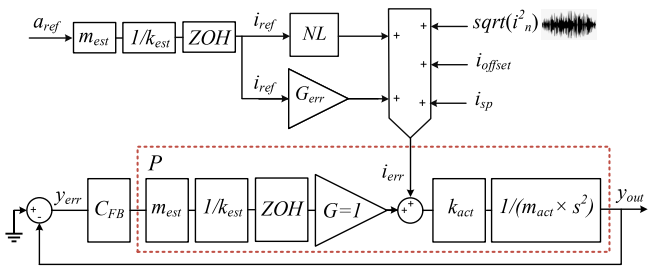

Fig. 4. Schematic outline of the sensitivity analysis model.

position errors, and for instance to achieve 2 nm-node technology, the power amplifier current drift should not exceed 1 mA/A.

Nonlinearity: As nonlinearity can have different shapes, it sounds more complicated to investigate. Following the approach in [10], a dimensionless spatial frequency $f_{spatial}$ is defined for calculating the nonlinear components as odd and even functions of i_{ref}:

$$\begin{aligned} i_{nonlin,even} &= I_{NL} \cos(2\pi f_{spatial} \frac{i_{ref}}{I_{\max}}) \\ i_{nonlin,odd} &= I_{NL} \sin(2\pi f_{spatial} \frac{i_{ref}}{I_{\max}}), \end{aligned} \tag{7}$$

where I_{NL} and $I_{\max}$ are the nonlinearity current amplitude and the applicable current range, respectively. For $f_{spatial}$ ranging from 0 A/A to 30 A/A and $I_{NL} = 0.01$ A, both odd and even nonlinearity error functions are simulated, and the respective graphs are shown in Fig. 5 (b)-(c). The peak value of the MRMS error related to odd nonlinearity occurs around $f_{spatial} = 3$ A/A, and for even nonlinearity MRMS increases as $f_{spatial}$ rises to 30 A/A. These results show that some shapes of nonlinearity cause larger errors. Thus, for analyzing the power amplifier performance, Total Harmonic Distortion (THD) is not a comprehensive comparison metric as it is possible that different shapes of nonlinearity with the same THD cause different amounts of MRMS errors. Hence, to obtain a thorough vision of the amplifier nonlinearity effect on the system, a sufficient number of the nonlinear signal harmonics should be included in the nonlinearity analysis.

Noise error: For the evaluation of noise error, the response of the system to an output current white noise error with a normal distribution is obtained. Since noise values are frequency dependent, and the position system response to the noise error is significant only for a limited frequency range, for this work to 20 kHz, noise calculations are done in the frequency domain and for the frequencies up to 20 kHz. Fig. 5 (d) illustrates the Cumulative Spectral Densisity (CSD) of MA, MSD and MRMS position errors for a 10 $\mu A/\sqrt{Hz}$ output current white noise error and frequencies up to 20 kHz. According to this figure, MA values are higher in lower frequencies, and thus MRMS is almost equal to MA for the low frequency range. On the other hand, MSD contains the high frequency part of error, and hence MRMS is approximately equal to MSD in this range. As Fig. 5 (e) shows, the current

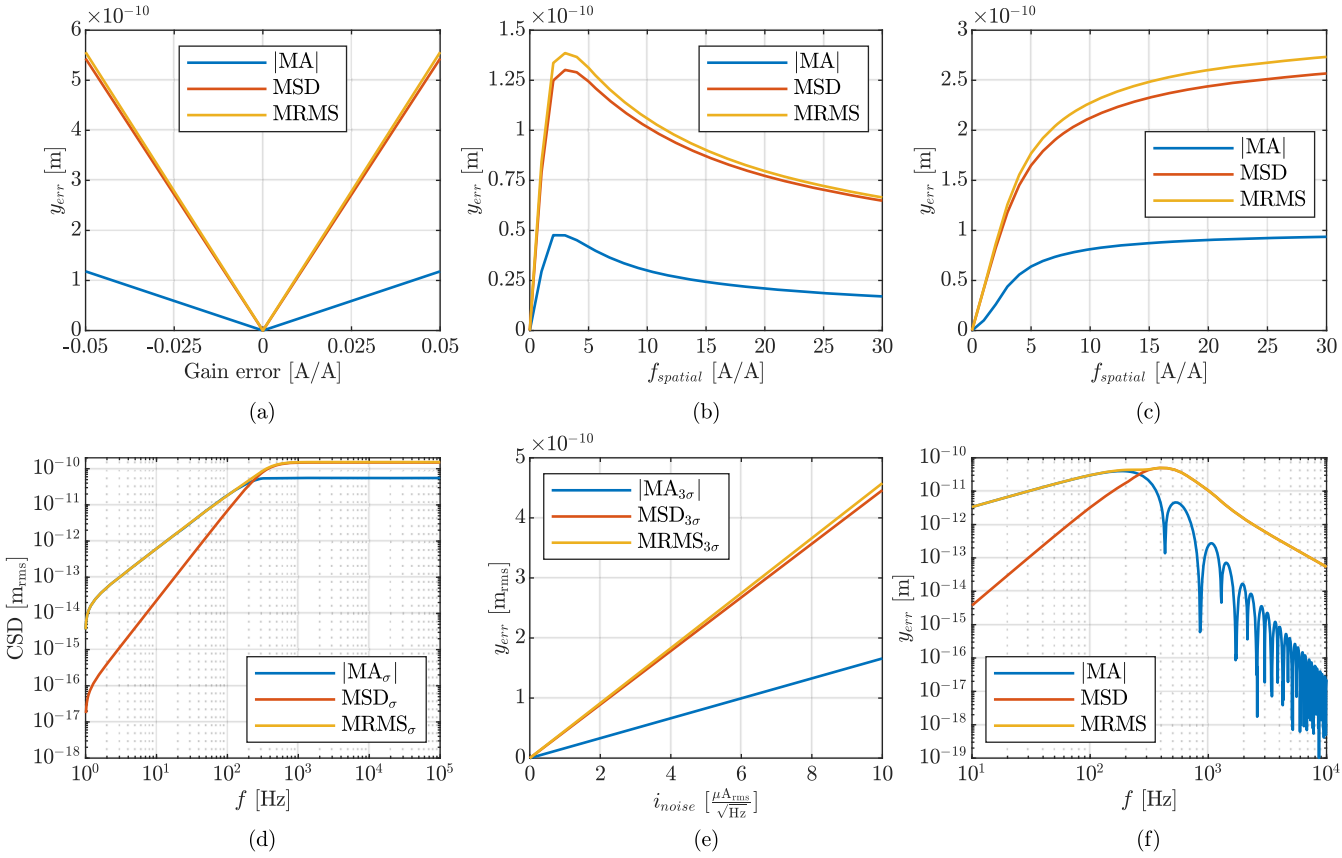

Fig. 5. Position errors versus (a) power amplifier gain drift, (b) odd nonlinearity, and (c) even nonlinearity; (d) CSD of position errors versus frequency for 10 μA/$\sqrt{\text{Hz}}$ current white noise error; (e) 3σ values of position errors versus current white noise error; (f) position errors for a spurious signal with 100 μA amplitude and frequency ranging from 10 Hz to 10 kHz.

noise, which mainly stems from the current sensor noise, considerably affects the position loop system performance. Again for the 2 nm example, the maximum output current white noise should be limited to 0.5 μA/$\sqrt{\text{Hz}}$.

Spurious signals: Any unwanted signal produced by the power amplifier outside the frequency band of interest can be called a spurious signal. In this paper, for analyzing the spurious signals, a sinusoidal error signal with 100 μA amplitude and frequency ranging from 10 Hz to 10 kHz is introduced to the position system shown in Fig. 4, and the generated MA, MSD, and MRMS position errors are calculated and represented in Fig. 5 (f). The position loop is more sensitive to signals within the $100-600$ Hz frequency range, and the peak MRMS occurs around 400 Hz. Therefore, spurious signals caused by the power line harmonics falling into this frequency range should be avoided. Also, MA is dominant for low frequency signals while MSD dominates in higher frequencies. Moreover, the power amplifier carrier signal can be treated as a spurious signal, and as Fig. 5 (f) illustrates, the higher the switching frequency of the carrier signal, the lower the sensitivity of the position loop to the PWM signals. For example, for $f_{s,cur} = 400$ kHz, if the amplitude of the carrier main harmonic is 1 mA, the calculated MRMS will be at the order of 10^{-22} m.

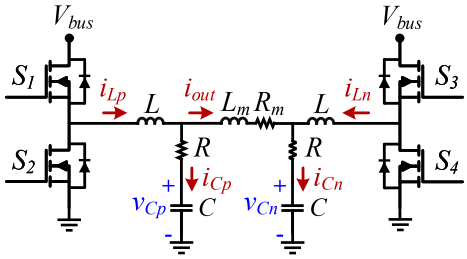

Fig. 6. Schematic of the simulated power amplifier.

IV. Controlled Current Loop Errors

In this section, a closed-loop controlled power amplifier is introduced to investigate its contribution to the position error of the motion system. The power amplifier is controlled by two cascaded current controllers, which aim to attain fast tracking and good stationary performance. In order to realize the real-time digital implementation, the current controllers are discretized with the sampling frequency of $f_{s,cur} = 400$ kHz.

Power amplifier topology: Fig. 6 presents the schematic of the power amplifier, where the output current i_{out} is used to actuate the motor [3]. This power amplifier has four operation modes in total with respect to the switching states (S_1, S_2, S_3, S_4). The averaged continuous state-space model of the power amplifier is derived for controller design [11]. The system states are $x = [i_{Lp} \quad v_{Cp} \quad i_{Ln} \quad v_{Cn} \quad i_{out}]^T$, and they are all considered measurable for simulation. The system inputs are the two duty-cycles of the two legs which are defined as $u = [d_p \quad d_n]^T$. The averaged model can be represented as $\dot{x}(t) = A_c x(t) + B_c u(t)$ and $y(t) = x(t)$, where

$$A_c = \begin{bmatrix} -\frac{R}{L} & -\frac{1}{L} & 0 & 0 & \frac{R}{L} \\ \frac{1}{C} & 0 & 0 & 0 & -\frac{1}{C} \\ 0 & 0 & -\frac{R}{L} & -\frac{1}{L} & -\frac{R}{L} \\ 0 & 0 & \frac{1}{C} & 0 & \frac{1}{C} \\ \frac{R}{L_m} & \frac{1}{L_m} & -\frac{R}{L_m} & -\frac{1}{L_m} & -\frac{2R+R_m}{L_m} \end{bmatrix}, \quad (8)$$

$$B_c = \begin{bmatrix} \frac{V_{bus}}{L} & 0 & 0 & 0 & 0 \\ 0 & 0 & \frac{V_{bus}}{L} & 0 & 0 \end{bmatrix}^T.$$

The averaged model (8) is discretized with the sampling frequency $f_{s,cur}$ for the current controller design. The discretized averaged model is denoted as $x(k+1) = Ax(k) + Bu(k)$ and $y(k) = x(k)$.

Cascaded controller: In [12], a power amplifier with a similar schematic to Fig. 6 was considered. The cascaded control configuration for the power amplifier is demonstrated in Fig. 1. For the inner loop (blue block), a linear quadratic regulator (LQR) is designed to improve the transient response. Then, an output feedback controller (OFC) in the outer loop is designed to achieve frequency specifications, which is a frequency loop shaping controller.

Linear quadratic regulator: At steady-state, the reference states x_s and reference inputs u_s can be calculated from the reference output current i_{ref} as $x_s = M_x i_{ref} + N_x$ and $u_s = M_u i_{ref} + N_u$, where $M_x = \begin{bmatrix} 1 & \frac{R_m}{2} & -1 & \frac{R_m}{2} & 1 \end{bmatrix}^T$, $N_x = \begin{bmatrix} 0 & \frac{V_{bus}}{2} & 0 & \frac{V_{bus}}{2} & 0 \end{bmatrix}^T$, $M_u = \begin{bmatrix} \frac{R_m}{2V_{bus}} & -\frac{R_m}{2V_{bus}} \end{bmatrix}^T$ and $N_u = \begin{bmatrix} \frac{1}{2} & \frac{1}{2} \end{bmatrix}^T$. The LQR controller is designed to minimize the following cost function:

$$J = \sum_{i=0}^{\infty} [(x(i) - x_s)^T Q (x(i) - x_s) + (u(i) - u_s)^T R (u(i) - u_s)], \quad (9)$$

where Q and R are weighting matrices. The Q and R are tuned by sampled data search, the position error is evaluated for different combinations of Q and R. The case which gives the least position error is selected as the optimal controller parameter. The optimal feedback gain K can be calculated by solving the corresponding discrete-time algebraic Riccati equation (e.g., using the dlqr function in Matlab). The optimal control input $u^*(x(k))$ is then calculated as $u^*(x(k)) = K(x(k) - x_s) + u_s$.

Output feedback controller: In order to design the output feedback controller, the inner closed-loop with the LQR controller and the amplifier model can be employed as a single input single output (SISO) system. As shown in Fig. 1, the system input is r_o and the system output is i_o. The inner closed-loop system is modelled as

$$\begin{aligned} x(k+1) &= Ax(k) + Bu(k) \\ &= Ax(k) + B\left(K\left(x(k) - x_s(k)\right) + u_s(k)\right) \\ &= (A + BK)x(k) + (BM_u - BKM_x)\, r_o(k) \\ &\quad + BN_u - BKN_x, \\ y(k) &= \begin{bmatrix} 0 & 0 & 0 & 0 & 1 \end{bmatrix} x(k). \end{aligned} \quad (10)$$

The OFC is designed to improve the bandwidth of the current loop using the loop shaping method based on the model (10). The design target is to achieve a bandwidth of at least 5 kHz for stationary performance. Its continuous-time transfer function is

$$C_{OFC}(s) = \frac{48.69s^2 + 6.003 \cdot 10^5 s + 3.887 \cdot 10^9}{s^2}. \quad (11)$$

$C_{OFC}(s)$ consists of two pure integrators and two conjugated zeros. This transfer function is discretized using the ZOH method with $f_{s,cur}$ for digital implementation.

Position error: The simulation is performed based on Fig. 1, and the PA dynamic model controlled by the described cascaded current controllers is included. Fig. 7 illustrates the evaluation of the position error using the controlled amplifier circuit, where the amplifier circuit is modelled using Simulink and Simscape. The position error gets largely increased when the ideal amplifier model is replaced with the controlled realistic amplifier circuit. The MSD error still dominates the position error.

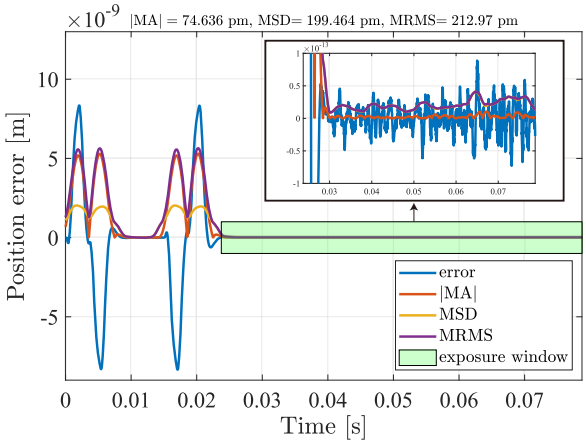

Fig. 7. Evaluation of the position error during the exposure window (controlled amplifier circuit).

Delay compensation: The largely increased position error can be regarded as an extra delay effect of the controlled current loop. In order to compensate for this delay, an interpolating delay block $(1 - \alpha) + \alpha^{-1}$ is connected in series with $C_{FF}(z)$ in the feedforward loop (Fig. 1), which enables the realization of the fractional delay tuning [10]. Fig. 8 shows the results of MA, MSD and MRMS position errors when the fractional number α varies from 0 to 1. The MRMS error

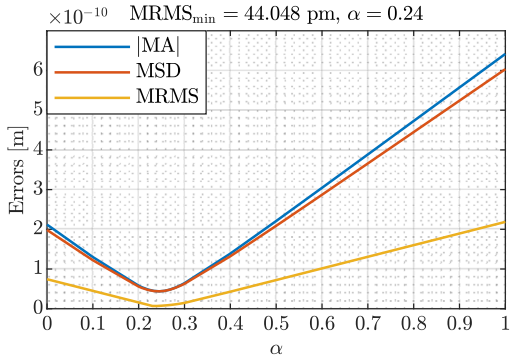

Fig. 8. MA, MSD and MRMS position error versus compensated delay.

can be minimized to the level of 44 pm by compensating the extra delay, and the fractional number that results in the optimal error is 0.24. Thus, it can be concluded that the extra delay caused by the controlled current loop is around $\frac{0.24}{f_{s,cur}} = 0.6\,\mu s$.

V. Conclusions

This research has analyzed the effects of power amplifier imperfections on a high-precision position system by using a complete mechatronics model which considers control, mechanical and electrical aspects. The analyzed errors have been divided in two categories: 1. additive errors and 2. current control errors. For studying the effects of additive errors including gain error, gain offset, nonlinearity, spurious signals, and noise error, a sensitivity analysis has been applied. As (6) shows, the sensitivity function has a direct and an inverse relationship with k_{act} and m_{act}, respectively. As the actuator mass increases or the actuator constant decreases, the position loop displays lower sensitivity to power amplifier additive errors. Also, nonlinearity analysis illustrates that THD is not a comprehensive comparison metric as it is possible that different shapes of nonlinearity with the same THD cause different amounts of MRMS errors. For investigating the current loop errors, a cascaded current controller has been considered for the power amplifier to realize how the system can be improved by modifying the control strategy, and a fractional delay has been added to the position loop feed-forward path to compensate for the observed delay between the position loop and the current loop. We demonstrated that the position system's MRMS can be improved by a factor of five by appropriately tuning the delay compensation in the feedforward path and the cascaded current control design. In the future, a more precise motion control system structure will be considered, which includes the resonance and non-linearity of the electromechanical plant. Sampled data control system analysis can be employed to investigate the difference between static characteristics and transient characteristics. Also, the power amplifier circuit can be included in the model to evaluate other error contributors such as dead time and the turn-on and turn-off characteristics of power semiconductors. As the developed method is applicable to any precision positioning system, a suggestion for future research is to modify the accuracy comparison metrics MA, MSD, and MRMS to fit any specific positioning system such as position-controlled robots, wire bonders, or 3D printers, and try to improve the position accuracy by tuning the delay compensation in the feedforward path.

Acknowledgment

This project has received from ECSEL Joint Undertaking (JU) under grant agreement No 875999. The JU receives support from the European Union's Horizon 2020 research and Innovation programme and the Netherlands, France, Germany, Austria, Israel, Belgium, Hungary, Romania and UK.

References

[1] T. Oomen, "Advanced motion control for precision mechatronics: control identification and learning of complex systems", IEEJ Journal of Industry Applications, vol. 7, no. 2, pp. 127-140, 2018, https://doi.org/10.1541/ieejjia.7.127.

[2] H. Butler, "Position control in lithographic equipment [applications of control]," in IEEE Control Systems Magazine, vol. 31, no. 5, pp. 28-47, Oct. 2011, doi: 10.1109/MCS.2011.941882.

[3] R.-H. M. Schmidt, "Ultra-precision engineering in lithographic exposure equipment for the semiconductor industry." Philos. Trans. A. Math. Phys. Eng. Sci., vol. 370, no. 1973, pp. 3950–72, 2012.

[4] J. M. Schellekens, H. Huisman, J. L. Duarte, M. A. M. Hendrix and E. A. Lomonova, "An analysis of the highly linear transfer characteristics of dual-buck converters," in IEEE Transactions on Industrial Electronics, vol. 65, no. 6, pp. 4681-4690, June 2018, doi: 10.1109/TIE.2017.2772175.

[5] M. Mauerer, A. Tüysüz and J. W. Kolar, "Distortion analysis of low-THD/high-bandwidth GaN/SiC class-D amplifier power stages," 2015 IEEE Energy Conversion Congress and Exposition (ECCE), 2015, pp. 2563-2571, doi: 10.1109/ECCE.2015.7310020.

[6] J. M. Schellekens, R. A. M. Bierbooms and J. L. Duarte, "Dead-time compensation for PWM amplifiers using simple feed-forward techniques," The XIX International Conference on Electrical Machines - ICEM 2010, 2010, pp. 1-6, doi: 10.1109/ICELMACH.2010.5608022.

[7] Q. Yu, E. Lemmen, C. G. E. Wijnands and B. Vermulst, "Output spectrum modelling of an H-bridge inverter with dead-time based on switching mode analysis," in IEEE Transactions on Power Electronics, early access, doi: 10.1109/TPEL.2021.3067638.

[8] B. J. D. Vermulst, "Compensating baseband distortion of regularly sampled pulsewidth modulators for high-precision power converters," in IEEE Transactions on Power Electronics, vol. 34, no. 7, pp. 6257-6263, July 2019, doi: 10.1109/TPEL.2018.2874362.

[9] K. W. Verkerk, H. Butler and P. P. J. van den Bosch, "Improved disturbance rejection for high precision systems through estimation of the flexible modes," 2015 IEEE Conference on Control Applications (CCA), 2015, pp. 1191-1196, doi: 10.1109/CCA.2015.7320774.

[10] S. J. Settels, J. van Duivenbode and J. L. Duarte, "Impact of amplifier errors on position loop accuracy of high-precision moving stages," 2017 19th European Conference on Power Electronics and Applications (EPE'17 ECCE Europe), 2017, pp. P.1-P.10, doi: 10.23919/EPE17ECCEEurope.2017.8099009.

[11] R.C.P. Leyva, A. Alonso, C. Queinnec, T. Isabelle, S. Martinez-Salamero, L.. (2006). Passivity-based integral control of a boost converter for large-signal stability. Control Theory and Applications, IEE Proceedings -. 153. 139 - 146. 10.1049/ip-cta:20045223.

[12] F. A. Qureshi, V. Spinu, K. Wijnands and M. Lazar, "A real-time control system architecture for industrial power amplifiers," 2013 American Control Conference, 2013, pp. 4510-4515, doi: 10.1109/ACC.2013.6580534.